Journal of Materials Science: Materials in Electronics (2019) 30:18374–18383
https://doi.org/10.1007/s10854-019-02191-2

# Electrical properties of $Zn_{(1-x)}Co_xO$ dilute magnetic semiconductor nanoparticles

**Kapil Y. Salkar[1] · R. B. Tangsali[1] · R. S. Gad[2] · Asnit Gangwar[3] · N. K. Prasad[3]**

Received: 10 July 2019 / Accepted: 11 September 2019 / Published online: 19 September 2019


**Abstract**
$Zn_{(1-x)}Co_xO$ nanoparticles with ($x = 0.05$, 0.10, 0.15 and 0.20) were prepared by combustion method. Here we report our findings on electrical properties carried out on these materials from room temperature to 500 °C. Thermopower investigations carried out on the materials resulted in Seebeck coefficient showing a transition from positive to negative values with '$x$' dependent enhancements. The material that exhibits a p-type semiconductor character at room temperature translates into an n-type of semiconductor at higher temperatures beyond 90 °C marked by a first order transition. Electrical resistivity and the activation energy being interrelated are seen to decrease with rising temperature due to increase in charge carrier concentration. Dielectric constant (ε) and dielectric loss (tan δ) investigated as a function of frequency showed nearly exponential decline in their values with increasing frequency for all the samples. However temperature dependent 'ε' and 'tan δ' show a peaking behaviour at lower temperatures with increasing trend at higher temperature as a result of increase in dielectric polarization. The DMS materials being ferromagnetic at room temperature are good temperature dependent semiconductors with high dielectric constant.

## 1 Introduction

Dilute magnetic semiconductor (DMS) materials, the genesis of materials for spintronic applications have become materials of fundamental importance in current day materials science research. These materials simultaneously exhibit both semiconductor as well as moderate to mild ferromagnetic properties and therefore can be exploited for spintronic applications where in one can use both electron charge and electron spin for transfer of information [1]. These types of materials are acquired from semiconductor materials like ZnO, $In_2O_3$, CuO, $SnO_2$ by doping them with materials like Co, Ni, Mn, Fe and other rare earth materials like Gd, Er, Nd, Eu, Dy at low concentration [1, 2]. The major challenge and requirement for production of spintronic devices is preparation of magnetic semiconductors with spin polarized carriers essential for transportation and manipulation [3]. It is stipulated that spintronic devices enjoy several advantages over conventional electronic devices like minimal power consumption, quick data processing meaning data processing at higher speeds, improved integration capacity and stability useful in logic devices, spin light emitting diodes, memory devices etc. [4]. Reports indicate that enormous amount of research is being carried out on II–VI and III–V group semiconductors for production of dilute magnetic semiconductors [5, 6]. However, preparation of group II–VI semiconductors is relatively effortless as compared to preparation of group II–VI doped semiconductors [7]. In case of group III–V semiconductor materials, GaMnAs is the most widely tested material with pitiable success in obtaining required room temperature ferromagnetism. Induction of room temperature ferromagnetism in materials like GaAs, InAs etc., and oxide based materials like $TiO_2$, $SnO_2$, $CeO_2$, ZnO etc., have been tried with trivial success [1, 3].

Among II–VI group semiconductors Zinc Oxide (ZnO) is a resourceful compound having large excitonic binding energy of 60 meV with direct band gap of 3.37 eV at room temperature [7, 8]. ZnO is being perceived as a future DMS material due to its massive potential, unique physical, optical, electronic, and chemical properties that are suitable for invention of electronics and optoelectronic nanoscale

✉ R. B. Tangsali
rbtangsali@unigoa.ac.in

[1] Department of Physics, Goa University, Taleigao Plateau 403206, Goa, India

[2] Department of Electronics, Goa University, Taleigao Plateau 403206, Goa, India

[3] Department of Metallurgical Engineering, IIT Banaras Hindu University, Varanasi 221005, India

devices. ZnO has wide ranging applications in drug delivery and bio-imaging, as well as fabrication of biosensors, solar cell, chemical gas sensors, light emitting diodes and field effect transistors [9, 10].

Electrical properties in transition (Fe, Mn, Ni, Co, Cr) metal doped ZnO, has been an exhilarating topic being investigated by researchers since last few years. Investigations reported on resistivity suggest that there is an increase in resistivity and activation energy due to reduction in grain growth and particle size with increasing Cobalt content in the ZnO matrix [12, 13]. Sajid Ali Ansari et al. (2012) have carried out investigations on dielectric properties of these materials and have explained the decrease in the dielectric constant with frequency on the basis of Koop's theory of space charge polarization whereas variation of dielectric constant with temperature is attributed to increase in charge carrier mobility due to thermal activation and rise of hopping frequency. The overall dielectric constant values with respect to frequency and temperature showed a decreasing trend with increasing Co concentration in the ZnO matrix [11]. However most of these studies are based on samples obtained using complex methods of sample preparation that do not produce monophasic material with higher level of Co concentration.

In our previous studies we have reported the preparation characterization and magnetic properties of $Zn_{(1-x)}Co_xO$ nanoparticle synthesized using auto-combustion method. Structural investigations showed formation of monophasic material with lattice constants '*a*' and '*c*' increasing and the average crystallite size decreasing from 25 to 17 nm on enhancement of Co content in the sample. The FT-IR spectra provided information on the absorption bands in the range of 400–576 $cm^{-1}$ which were due to Zn–O and Co–O stretching bonds in the samples. Scanning electron microscope (SEM) micrographs showed agglomerates of nanoparticles and Energy dispersive spectroscopy (EDS) spectra provided the molecular weight percentage $1-x$ of Zn and $x$ of Co as well as molecular weight percentage of O. These values of molecular weight percentages were in good agreement with the theoretically calculated molecular weight percentages of Zn, Co and O [14]. Magnetic measurements such as hysteresis, field cooled and zero field cooled (FC and ZFC) made on the samples confirmed presence of room temperature ferromagnetic phase in the materials. Energy band gap obtained from UV spectra showed decreasing trend with increasing $Co^{2+}$ content in the sample. Photoluminescence studies carried out on the samples showed several emission peaks ranging from green to violet emissions with different luminescence decay times [14].

In the present article we report interesting findings on electrical properties of monophasic Co-doped ZnO nanoparticles. Electrical properties such as thermoelectric power, DC resistivity, Dielectric constant (ε), dielectric loss (tan δ) were investigated for all the Co doped samples. Temperature dependence of Seebeck coefficient suggests p-type semiconductor behaviour for the material at room temperature that transforms into n-type semiconductor with a first order transition at higher temperatures. The DC resistivity and activation energy decreases irrespective of reduction in grain growth and particle size with increasing $Co^{2+}$ content in the samples. Investigation on dielectric properties showed that increase of $Co^{2+}$ ions in ZnO matrix enhances the dielectric constant with induction of relaxation process in the lower temperature range.

## 2 Material preparation and investigation techniques

The material preparation of Co-doped ZnO dilute magnetic semiconductor nanoparticles was carried out as described in our earlier work [14]. Thermopower in the range of room temperature to 500 °C was measured using DOSE-Thermopower 16 bit RISC microcontroller with 16-bit A/D converter. Variation of DC resistivity with temperature in the range of 303–773 K was measured using two probe setup. Dielectric constant (ε) and Dielectric loss (tan δ) as a function of applied frequency in the range of 20 Hz to 3 MHz and temperature in the range of 303–773 K was obtained using Wayne Kerr precision component analyzer 6440B.

## 3 Result and discussion

### 3.1 Thermoelectric properties

The plots given in Fig. 1a shows the variation of Seebeck coefficient 'S' (V/K) with 'T' (°C) the temperature of hot junction for all the samples. The Seebeck coefficient 'S' was calculated using Eq. (1) and the charge carrier concentrations at different temperatures were calculated using Eq. (2) and (3).

$$S = \frac{\Delta V}{\Delta T} \tag{1}$$

$$n = 2\left(\frac{2\pi m_e KT}{h^2}\right)^{3/2} \exp\left[-\frac{(E_c - E_f)}{KT}\right] \tag{2}$$

$$p = 2\left(\frac{2\pi m_h KT}{h^2}\right)^{3/2} \exp\left[-\frac{(E_f - E_v)}{KT}\right] \tag{3}$$

In Eqs. (1–3) ΔV is the thermo-electro motive force (emf), ΔT is temperature difference across hot and the cold

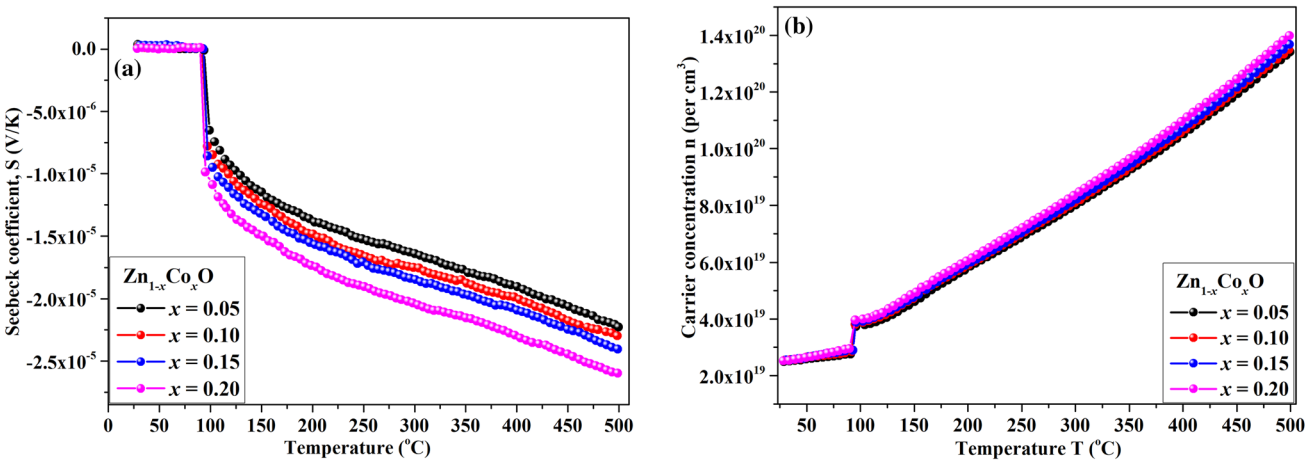


**Fig. 1** **a** Variation of Seebeck coefficient with temperature and **b** variation of Carrier concentration with temperature for $Zn_{(1-x)}Co_xO$ with $x = 0.05$, 0.10, 0.15 and 0.20

junction, '$m_h$' and '$m_e$' are the rest mass of the carriers (holes and electron), 'K' is the Boltzmann constant, '*h*' is the Planck's constant and 'S' is the Seebeck coefficient. $E_c$ is the bottom energy level of the conduction band, $E_v$ is the upper energy level of the valence band and $E_f$ is the position of the fermi energy level. The polarity sign of the Seebeck coefficient designates the nature of the charge carriers (holes or electron) and also gives information about the material type (p-type or n-type) [15]. It can be seen that the Seebeck coefficient 'S' has a positive value at room temperature which remains almost constant for lower temperature range up to a temperature of 90 °C representing a p-type semiconductor behaviour of all the samples. However there is a marginal rise in carrier concentration in this temperature range as indicated in Fig. 1b. A first order charge polarity transition is observed at about 90 °C from p-type charge carriers to n-type charge carriers with substantial enhancement in n-type charge carrier concentration indicative of change in the type of semiconductor behaviour. Thus the samples behave like p-type semiconductors from room temperature to about 90 °C and n-type of semiconductors from 90 °C and above and perhaps beyond 500 °C which is the limitation of the equipment used for measurement, with electrons as majority of the charge carries engaged in conduction mechanism [15, 16]. Figure 1b gives a plot of charge carrier concentration versus temperature of hot junction. The carrier concentration increases from room temperature approximate value of $2.53 \times 10^{19}$ per $cm^3$ to a value of $1.35 \times 10^{20}$ per $cm^3$ at 500 °C. At elevated temperature electrons are thermally activated called as conduction electrons which play a crucial role in Seebeck coefficient. It is observed that the Seebeck coefficient value reduces for all the $Co^{2+}$ concentration with increase in carrier concentration. At elevated temperatures charge carriers (electrons) are thermally activated which gain enough energy to hop from valance band to the conduction band. Enhancement of charge carriers (electrons) in the conduction band increases the charge carrier collisions which results in subordinating the 'S' values [17].

## 3.2 DC resistivity

An electrical resistivity is a measure of how sturdily the material opposes the flow of electric current in itself whereas electrical transport mechanism gives the significant information about the conduction mechanism in material. Figure 2a shows the plots of $\log_{10} \rho$ (Ω cm) v/s 1000/T ($K^{-1}$) for the samples. The resistivity 'ρ' for the samples at different temperature was calculated using Eq. (4).

$$\rho = \left(\frac{VA}{It}\right) \tag{4}$$

where 'V' is applied voltage across the sample, 'A' is cross-sectional area of the pallet, 'I' is current and 't' is thickness of the pallet. The log resistivity plots in Fig. 2a can be divided into three different regions over the temperature range of 303–773 K. The first region I is between 303 and 363 K, region-II between 363 and 398 K and region-III is between 398 and 773 K respectively. It may be seen that in region I the resistivity shows a small increment as temperature is increased from room temperature to 363 K. Normally increase in resistivity in this region is attributed to setting up of phonon vibrations that scatter charge carriers which results in reduction of mean free path of the free charge carriers [18, 19]. However in materials under investigation it appears that the increase in resistivity due to phonon vibration is very much less compared to reported results on similar materials [20, 21]. This means that either the charge carriers are less in number at these temperatures or phonon vibrations are not very strong to bring about large number

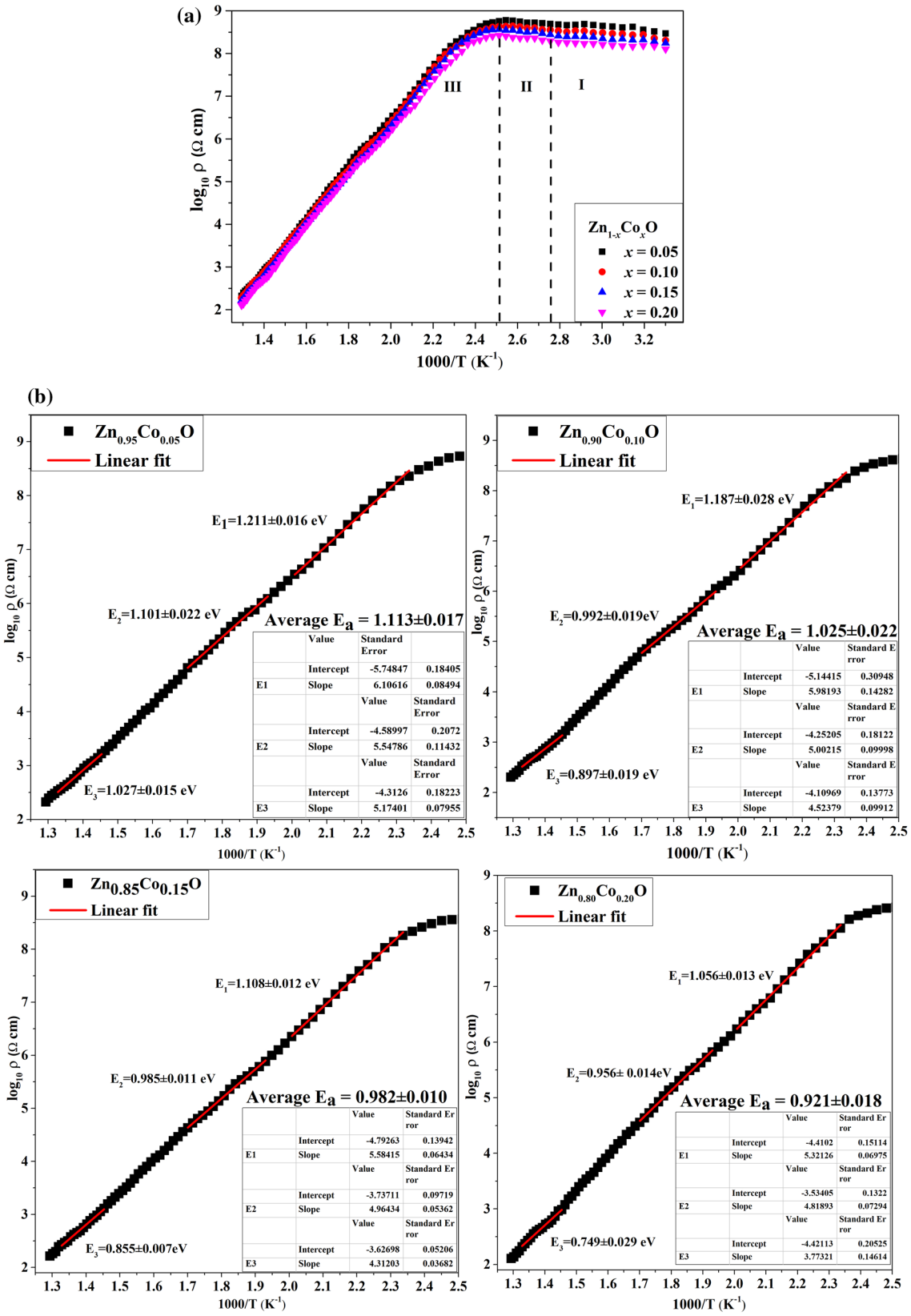


**Fig. 2** **a** Variation of resistivity with temperature and **b** Arrhenius plot at high temperature region (398 K to 773 K) for $Zn_{(1-x)}Co_xO$ with $x = 0.05$, 0.10, 0.15 and 0.20

of multiple charge carrier scatterings. Since the material exhibits large values of resistivity of the order larger than $10^8$ Ω cm and above, it means that not many free charge carriers are available for conduction in this region. Moreover a look at low temperature thermopower Fig. 1a shows that from room temperature to near about 90 °C the systems are dominated by positive charge carriers that are holes. Hole movement in semiconductors is different from that of electron motion. Hence phonons will not have much effect on conduction of holes in the semiconductor in this region. At about 90 °C there is a first order phase transition which can be clearly seen from the Seebeck coefficient and charge carrier concentration curves shown in Fig. 1. It appears that the thermal energy at this temperature is sufficient to empty large number of valance electrons into conduction band. The concentration of electrons at this temperature is of the order of $3.79\times10^{19}$ per $cm^3$ which is typically found in a semiconductor. With sufficient electron charge carriers in this temperature region II between 90 °C to about 125 °C phonons become active and their effect can be visualized in Fig. 2a as a minor rise in resistivity due charge carrier scattering. Beyond this region the thermal energy available for ejection of charges goes on increasing leading to enhancement of electron charge carrier population in the conduction band which results in steep fall of resistivity of the materials in region III as seen in Fig. 2a. From Fig. 1b it can be seen that the carrier concentration in region II rises slowly till the temperature reaches to about 125 °C. The charge carrier concentration in this region grows slowly after initial transition at 90 °C. This rise in carrier concentration increases more rapidly from an approximate value of $4.21\times10^{19}$ per $cm^3$at 125 °C to a value of $1.35\times10^{20}$ per $cm^3$ at 500 °C in region III. It may be seen that resistivity and thermopower are dependent on $Co^{2+}$ concentration in the sample. The resistivity shows a descent decrease whereas as thermo power and carrier concentration exhibits a increasing trend as $Co^{2+}$ concentration is increased from $x=0.05$ to $x=0.20$.

The Arrhenius equation provides the relation between the activation energy ($E_a$) and temperature dependent material resistivity. The activation energy for all the samples in region III (398–773 K) has been calculated using Arrhenius Eq. (5).

$$\rho = \rho_0 \exp\left(\frac{E_a}{K_\beta T}\right) \tag{5}$$

where ρ is the resistivity at temperature T, $\rho_o$ is the constant, $E_a$ is the activation energy and $k_\beta$ is the Boltzmann constant. Figure 2b shows the Arrhenius plot at high temperature region (398–773 K) for all the samples which is fitted linearly in order to obtain the activation energy ($E_a$). The activation energy as per the reports depends on the crystalline nature of the material (single crystal or poly-crystalline), crystallite size and the applied temperature wherein the which measurements are made [22, 23]. Normally for any semiconductor material, the activation energy is the energy that facilitates charges to hop from one region (valance band) to other (conduction band) [22, 24]. At high temperature large amount of thermal energy is available for the charge carriers which results in subordinating the activation energy [25]. These helps in accelerating the charge transfer mechanism as more and more electrons are moved into conduction band thereby reducing the resistivity of the material. This is evident from the activation energy calculations made at different temperatures between 398 and 773 K. Activation energy values ($E_a$) calculated around three different temperatures from the resistivity curves using Eq. (5) are shown in Fig. 3 with inset showing the average activation energy. It may be seen that ($E_a$) values decreases with increase in temperature which substantiates the fact mentioned earlier about reduction of activation energy with rising temperature. Figure 3 shows that the activation energy also keeps decreasing with increase of $Co^{2+}$concentration in the sample. This reduction in activation energy can be understood on the basis of band gap reduction on increase of $Co^{2+}$ concentration in the sample. It has been reported that the band gap reduces with increases in $Co^{2+}$ content in the sample [14]. Increase in $Co^{2+}$ in the material increases the donor carrier density in the sample thereby shifting the Fermi level closer to the conduction band. Hence the energy gap between the donor level and the conduction band keeps decreasing with increasing $Co^{2+}$ concentration in the sample [25, 26]. Therefore the energy required for the charge carriers in the valance band to hop into the conduction band goes on reducing. Thus excess charge carriers in the conduction band bring down the resistivity of the material from about $2.95\times10^8$ Ω cm at room temperature to about $2.19\times10^2$ Ω cm at 773 K.

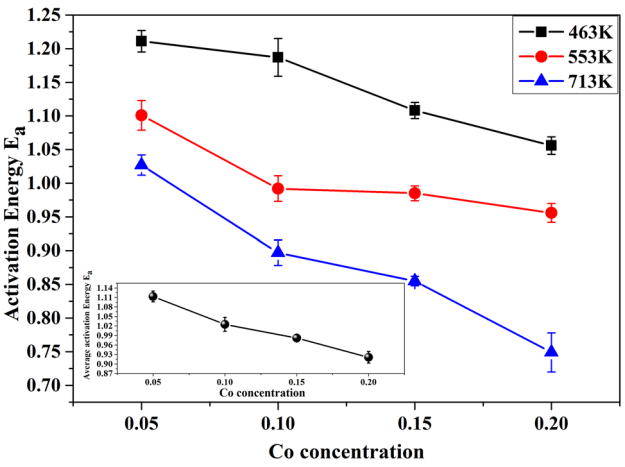


**Fig. 3** Variation of activation energy '$E_a$' of $Zn_{(1-x)}Co_xO$ with Co concentration $x=0.05$, 0.10, 0.15 and 0.20 at temperatures 463 K, 553 K and 713 K

Figure 4 shows a plot of (Δρ/ΔT) that is variation of resistivity with variation in temperature at various $Co^{2+}$ concentrations in the sample and at various temperatures. It may be seen that Δρ/ΔT shows identical decreasing trends in all the plots indicating decrease in resistivity with increasing $Co^{2+}$ concentration in the sample at different temperature. From Table 1 it can be seen that Δρ/ΔT evaluated at 313 and 363 K are positive for all the given concentration, whereas the same are negative at 398, 463, 553 and 713 K for all the given concentration. Since all the plots of Δρ/ΔT exhibit identical trend it means that the fall of resistivity with temperature is identical for all $Co^{2+}$ concentrations.

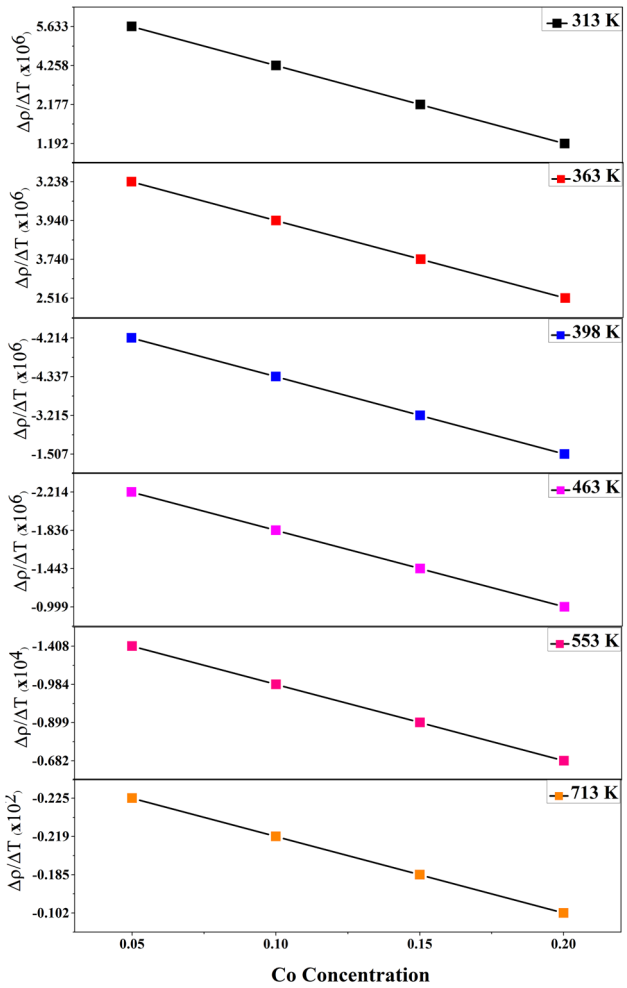


**Fig. 4** Variation of (Δρ/ΔT) with $Co^{2+}$ concentration in the sample at various temperatures

## 3.3 Frequency and temperature dependent dielectric properties

Figure 5a shows the variation of dielectric constant (ε) with frequency at room temperature of $Zn_{(1-x)}Co_xO$ with $x=0.05$, 0.10, 0.15 and 0.20 samples. The term dielectric constant (ε) expresses the energy storage in the dielectric material as polarization. The dielectric constant 'ε' was calculated using Eq. (6).

$$\varepsilon = \frac{Ct}{\varepsilon_0 A} \tag{6}$$

where, 'C' is the capacitance, 't' is the thickness of the pallet, 'A' is the area of the pallet and '$\varepsilon_0$' is the permittivity of free space [$\varepsilon_0 = 8.85 \times 10^{-14}$ (F/cm)]. It is observed that for all the $Co^{2+}$ concentrations dielectric constant 'ε' values initially decreases rapidly as the frequency increases and the further reduces very slowly on increasing the frequency. This decreasing behaviour in dielectric constant with frequency can be elucidated on the basis of Maxwell–Wagner model of interfacial polarization which is in agreement with Koop's phenomenological theory [27]. According to this model, dielectric medium is presumed to be made-up of fine conducting grains which are detached with poor conducting grain boundaries. In presence of applied external electric field, charge carriers with opposite polarity move inside the grain in opposite directions. The migrant charges gather at the grain boundaries due to separation of poor conducting grain boundaries. Therefore grains acts as an electric dipole in presence of applied external electric field, termed as interfacial polarization or space charge polarization. This form of electric polarization gives rise to high dielectric constant value at low frequency in general for all the samples [28, 29]. Inspection of dielectric constant with variation of '$x$' shows that the overall dielectric constant enhances as the $Co^{2+}$ concentration increases from $x=0.05$ to $x=0.20$. Increases of dielectric constant (ε) indicate enhancement of charge carrier density that is dependent on both frequency and induction of $Co^{2+}$ ions in the ZnO matrix. This is obvious as high values of dielectric constant are observed at both

**Table 1** Δρ/ΔT values at different temperature and $Co^{2+}$ concentrations

| Sample | 313 K (×10^6) | 363 K (×10^6) | 398 K (×10^6) | 463 K (×10^6) | 553 K (×10^4) | 713 K (×10^2) |
|---|---|---|---|---|---|---|
| $\frac{\Delta\rho}{\Delta T}$ | | | | | | |
| 0.05 | 5.633 | 3.238 | −4.214 | −2.214 | −1.408 | −0.225 |
| 0.10 | 4.258 | 3.940 | −4.337 | −1.836 | −0.984 | −0.219 |
| 0.15 | 2.177 | 3.740 | −3.215 | −1.443 | −0.899 | −0.185 |
| 0.20 | 1.192 | 2.516 | −1.507 | −0.999 | −0.682 | −0.102 |

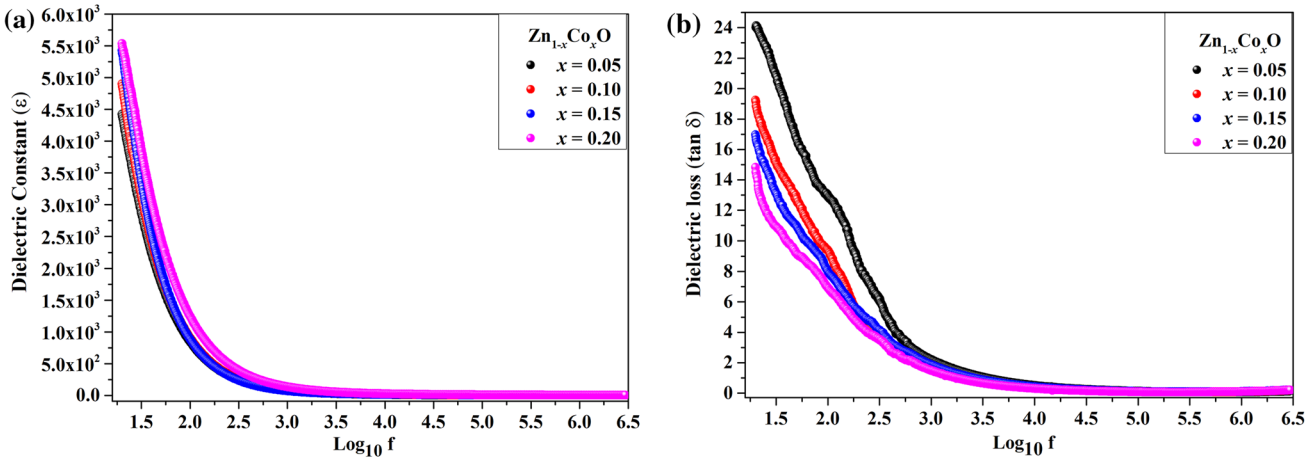


**Fig. 5** Variation of **a** dielectric constant (ε) and **b** dielectric loss (tan δ) with frequency at room temperature of $Zn_{(1-x)}Co_xO$ with $x=0.05$, 0.10, 0.15 and 0.20

lower frequencies as well as at higher $Co^{2+}$ concentrations. Moreover crystallite size is also known to play an important role in dielectric constant (ε) [30, 31]. Our previous structural analysis result shows reduction of crystallite size with increasing $Co^{2+}$ concentration in the material [14]. It is obvious that reduction in crystallite size would increase the number of crystallites per unit volume. As a result, there is an increase in dielectric constant of the material at low frequencies. Thus reduction in crystallite size amounts to increase in surface to volume ratio and an enhancement in over all grain boundary of the crystallites per unit volume. Thus increase in grain boundary and enrichment of charge carrier concentration due to increased $Co^{2+}$ concentration provides enhancement of dielectric constant at lower frequencies [32]. This value of high dielectric constant (ε) keeps falling as the frequency of electric field is increased. This may be attributed to the sluggishness of dipole orientations that cannot follow the high frequency of applied electric field which is related to the hopping rate of $Co^{2+}$ and $Zn^{2+}$ ions. Thus the contributing polarizability keeps lagging behind the applied external electric field at higher frequencies [27, 29].

Dielectric loss (tan δ) with respect to frequency at room temperature is shown in Fig. 5b. The dielectric loss signifies the dissipation or loss of energy in a dielectric material and it occurs when the polarization in a dielectric material lags behind the frequency of applied electric field. It is obvious that as the frequency increases the dielectric loss (tan δ) decreases swiftly and on further increasing the frequency tan δ shrinks very slowly, the variation in tan δ curves exhibits a declining trend similar to the dielectric constant. Generally, polar dielectrics molecules orient themselves in the direction of applied electric field which requires small amount of electric energy to overcome the internal forces. The rotation of dipole molecules and the movement of molecules from one site to another site in presence of applied electric field utilize a fraction of electric energy which leads to energy loss. It is clearly visible from the figure that dielectric loss is maximum for $x=0.05$ sample and minimum for $x=0.20$ sample at lower frequency. The dielectric loss in the dielectric material could be due to grain boundary effect (space charge polarization), crystallite size and hopping rate of the ions. Structural results given in our earlier report [14] indicate that crystallite size decreases with increasing $Co^{2+}$ content in the sample. Decrement in crystallite size with increasing $Co^{2+}$ content in the sample, raises the surface to volume ratio which increases the number of crystallites per unit volume thereby increasing the overall surface charge polarization. As a result energy required to orient the dipoles in the direction of electric field now depends on $Co^{2+}$ concentration in the sample and hence becomes lower at lower frequency for higher $Co^{2+}$ concentrations [18]. Although the sample with higher $Co^{2+}$ concentration shows lower grain size and higher dielectric constant, energy loss shown by tan δ curves in Fig. 5b goes on diminishing with increasing $Co^{2+}$ concentration in the samples due to reasons mentioned above. It may be seen that all tan δ curves exhibit a broad hump in the lower frequency region approximately between 100 Hz to about 350 Hz. Which may be viewed as a relaxation peak that smoothens reduces with increasing $Co^{2+}$ concentration. A relaxation peak is normally observed in materials in which charge carrier hopping frequency matches with the applied external electric field frequency [30]. Decreasing tan δ with frequency and $Co^{2+}$ concentrations in the sample suggests that these materials can be potentially used for spintronic applications in high frequency devices [33].

Dielectric constant of a dielectric material in addition to frequency is sensitive to temperature. Dielectric constant of all the samples has been recorded at different frequencies from room temperature to 500 °C. Variation

of dielectric constant with temperature of all the samples under investigation is presented in Fig. 6. It may be seen that all the samples initially show a peaking behaviour in the low temperatures between room temperature of 30 °C and 100 °C for all the frequencies. The peak is sensitive to frequency and the $Co^{2+}$ concentrations in the sample. Since crystallite size of these materials is dependent on $Co^{2+}$ concentration, which can be seen from our previous report [14] one can easily relate the magnitude of the peak height to the particle size of the material. The peaks known as relaxation peaks are frequency dependent as these are generated due to the relaxation time which is the time taken by the electric dipoles to get oriented in the applied electric field direction. When the relaxation time matches with the time period of the applied field, there is a resonance phenomenon wherein the sample absorbs maximum energy from the applied ac field. This can be seen from corresponding of dielectric loss v/s temperature curves given in Fig. 7. Since dielectric relaxation time is a characteristic of dielectric material, the spread being narrow, the peak height of both dielectric constant and dielectric loss falls as ac field frequency is increased and ultimately becomes flat at a higher frequency of 500 kHz. At lower temperature and high frequency the relaxation peak disappears as a result of charge carrier localization [11, 32]. But as the temperature increases the increased thermal energy increases charge carrier hopping rate resulting in increased charge carrier mobility thereby enhancing the conductivity of the material. Thus there is a large enhancement of dipole polarization which is dependent on applied frequency [11, 24], and $Co^{2+}$ concentrations in the material. The dielectric loss (tan δ) plots of Fig. 7 show identical trend to the one shown by dielectric constant plots in Fig. 6. Dielectric loss occurs when the dielectric polarization lags behind the applied electric field which is mainly due to grain boundary effect in the crystalline material. In case of nanoparticle sample the dielectric properties also depend on factors like the method of sample preparation, structure, crystallite size, chemical composition and preparative condition [24].

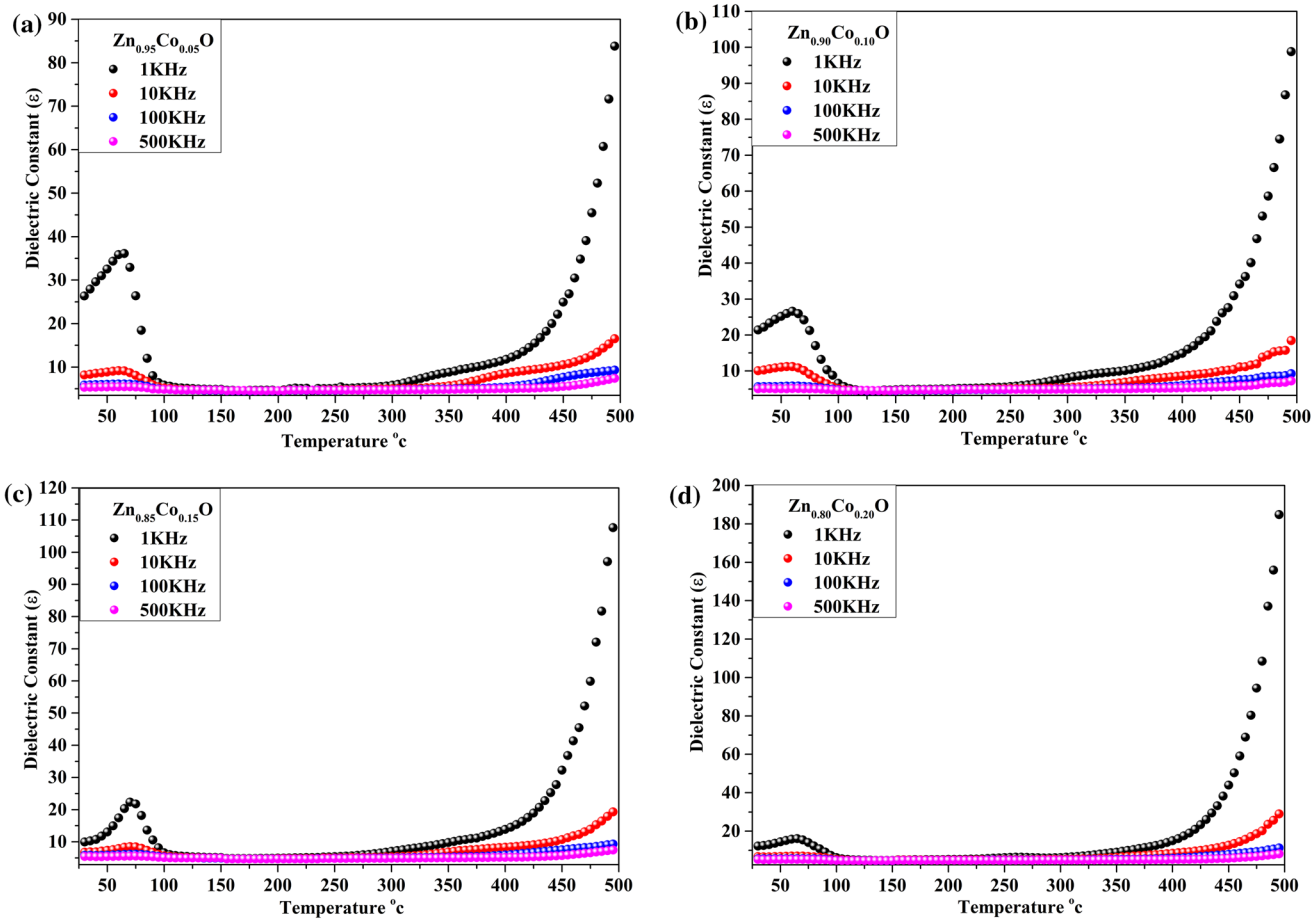


**Fig. 6** Variation of dielectric constant ('ε') as a function of temperature with different applied ac frequency for $Zn_{(1-x)}Co_xO$ with **a** $x=0.05$, **b** $x=0.10$, **c** $x=0.15$, **d** $x=0.20$

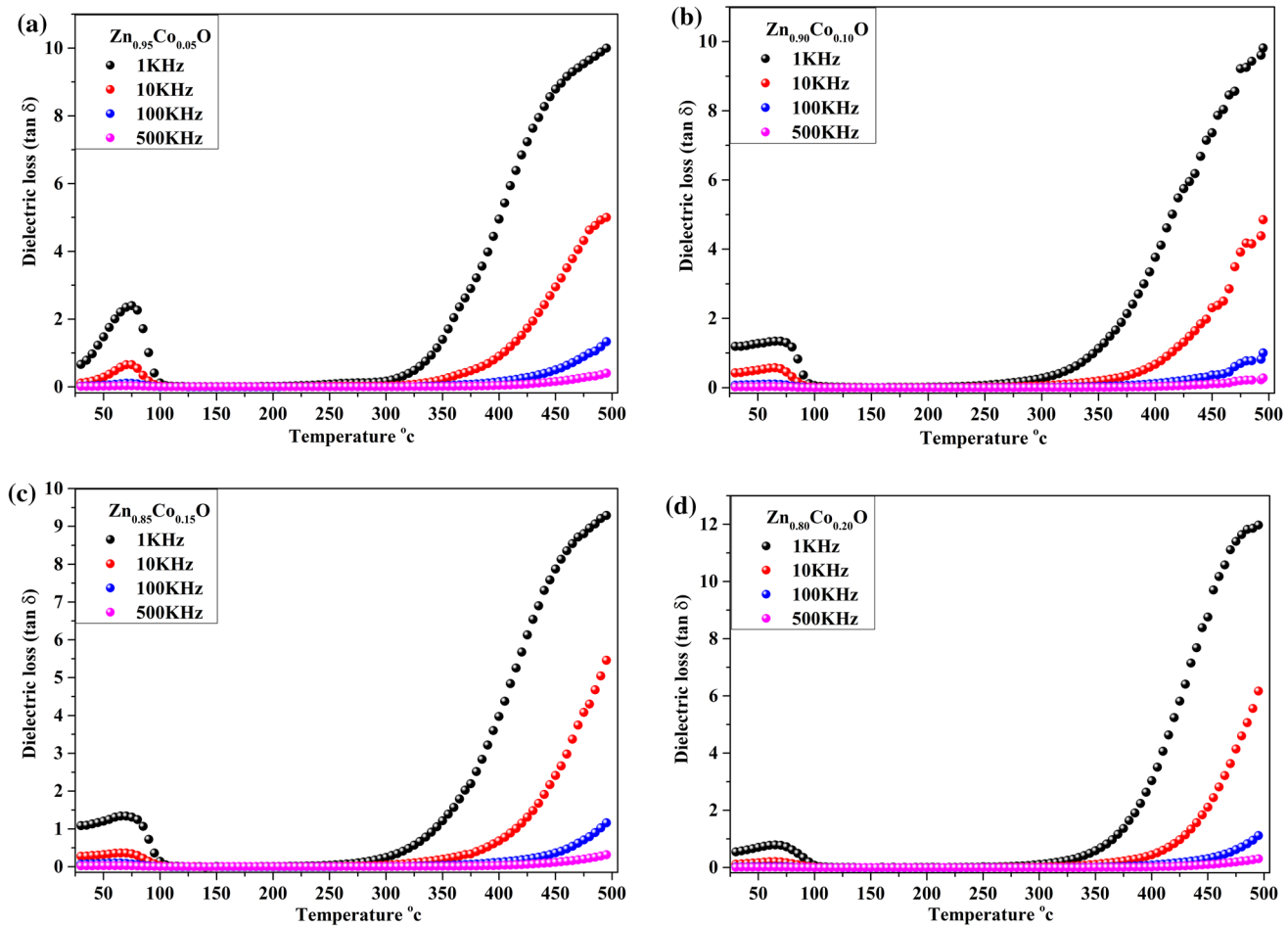


**Fig. 7** Variation of dielectric loss (tan δ) as a function of temperature with different applied ac frequency for $Zn_{(1-x)}Co_xO$ with **a** $x=0.05$, **b** $x=0.10$, **c** $x=0.15$, **d** $x=0.20$

## 4 Conclusion

Experimental investigations were carried out on monophasic $Zn_{1-x}Co_xO$ nanoparticle DMS materials with $x=0.05$, 0.10, 0.15, 0.20 prepared using combustion method, to understand their electrical properties. The analysis of Seebeck coefficient shows that all the materials behave like a dual type of semiconductor. All the nanoparticle samples exhibit p-type semiconductor character between room temperature to 90 °C and n-type semiconductor character at temperatures beyond 90 °C marked by a first order phase transition at 90 °C. DC resistivity was found to decreases with increase in temperature for all the samples exhibiting a semiconductor type of behaviour. In general the dielectric constant (ε) and dielectric loss (tan δ) showed a decreasing trend with increasing frequency; however it was sensitive to $Co^{2+}$ concentration. With increase in $Co^{2+}$concentration the dielectric constant (ε) was found to increase thereby lowering the dielectric loss (tan δ) due to enrichment of charge carriers in the ZnO matrix. Temperature dependent Dielectric constant (ε) and Dielectric loss (tan δ) shows similar variation with peaking behaviour at lower temperature due to relaxation phenomenon. The observed electrical properties provides a lucid evidence of inclusion of $Co^{2+}$ ions in high spin configuration that has strongly influenced the ZnO matrix giving reliable and remarkable results. Thus the investigation shows that a simple method like auto-combustion method of sample preparation could be successfully used to produce superior quality monophasic $Co^{2+}$ doped DMS material ensuring better electrical properties. The material with room temperature ferromagnetism, high dielectric constant can be used as a p-type of DMS material at lower temperatures and an n-type DMS material at higher temperatures beyond 90 °C.

## References

1. J. Cao, J. Wu, Strain effects in low-dimensional transition metal oxides. Mater. Sci. Eng. **71**, 35–52 (2011)

2. M. Mustaqima, C. Liu, Zno-based nanostructures for diluted magnetic semiconductor. Turk. J. Phys. **38**(3), 429–441 (2014)
3. G. Neumark, Y. Gong, I. Kuskovsky, Doping aspects of Zn-based wide-band-gap semiconductors. Handb. Electron. Photonic Mater (2007). https://doi.org/10.1007/978-0-387-29185-7_35
4. Z.L. Wang, Zinc oxide nanostructures: growth, properties and applications. J. Phys. **16**, 829–858 (2004)
5. Ü. Özgür, Ya.I. Alivov, C. Liu, A. Teke, M.A. Reshchikov, S. Doğan, V. Avrutin, S.-J. Cho, H. Morkoç, A comprehensive review of Zno materials and devices. J. Appl. Phys. **98**, 041301 (2005)
6. A. Moezzi, A.M. Mcdonagh, M.B. Cortie, Zinc oxide particles: synthesis, properties and applications. Chem. Eng. J. **185**, 1–22 (2012)
7. D.P. Norton, Y.W. Heo, M.P. Ivill, K. Ip, S.J. Pearton, M.F. Chrisholm, T. Steiner, ZnO growth doping and processing. Mater. Today **7**(6), 34–40 (2004)
8. J.S. Wellings, N.B. Chaure, S.N. Heavens, I.M. Dharmadasa, Growth and characterisation of electrodeposited Zno thin films. Thin Solid Films **516**(12), 3893–3898 (2008)
9. A.S.H. Hameed, C. Karthikeyan, S. Sasikumar, V.S. Kumar, S. Kumaresan, G. Ravi, Impact of alkaline metal ions $Mg^{2+,}$ $Ca^{2+}$, $Sr^{2+}$ and $Ba^{2+}$ on the structural, optical, thermal and antibacterial properties of Zno nanoparticles prepared by the co-precipitation method. J. Mater. Chem. B **1**(43), 5950–5962 (2013)
10. L. Schmidt-Mende, J.L. Macmanus-Driscoll, ZnO-nanostructures defects and devices. Mater. Today **10**(5), 40–48 (2007)
11. S.A. Ansari, A. Nisar, B. Fatma, W. Khan, M. Chaman, A. Azam, A.H. Naqvi, Temperature dependence anomalous dielectric relaxation in Co doped ZnO nanoparticles. Mater. Res. Bull. **47**(12), 4161–4168 (2012)
12. C.B. Fitzgerald, M. Venkatesan, J.G. Lunney, L.S. Dorneles, J.M.D. Coey, Cobalt-doped ZnO—a room temperature dilute magnetic semiconductor. Appl. Surf. Sci. **247**, 493–496 (2005)
13. U. Godavarti, V.D. Mote, M. Dasari, Role of cobalt doping on the electrical conductivity of ZnO nanoparticles. J. Asian Ceram. Soc. **5**(4), 391–396 (2017)
14. K.Y. Salkar, R.B. Tangsali, R.S. Gad, M. Jeyakanthan, U. Subramanian, Preparation characterization and magnetic properties of $Zn_{(1-x)}Co_xO$ nanoparticle dilute magnetic semiconductors. Superlattices Microstruct. **126**, 158–173 (2019)
15. M. Raghasudha, D. Ravinder, P. Veerasomaiah, Thermoelectric power studies of Co–Cr nano ferrites. J. Alloys Compd. **604**, 276–280 (2014)
16. M. Ohtaki, K. Araki, K. Yamamoto, High thermoelectric performance of dually doped ZnO ceramics. J. Electron. Mater. **38**(7), 1234–1238 (2009)
17. M. Ullah, W.B. Su, A. Manan, A.S. Ahmad, A.A. Shah, Z. Yao, Phase, microstructural investigation and thermoelectric properties of Ga doped zinc oxide-based ceramics sintered under an argon atmosphere. Ceram. Int. **44**(15), 17873–17877 (2018)
18. P.P. Naik, R.B. Tangsali, Enduring effect of rare earth ($Nd^{3+}$) doping and γ- radiation on electrical properties of nanoparticle manganese zinc ferrite. J. Alloy. Compd. **723**, 266–275 (2017)
19. A.R. Khantoul, M. Sebais, B. Rahal, B. Boudine, O. Halimi, Structural and optical properties of ZnO and Co doped ZnO thin films prepared by sol-gel. Acta Phys. Polon. A **133**, 114–117 (2018)
20. A.D. Acharya, B. Sarwan, R. Panda, S.B. Shrivastava, V. Ganesan, Tuning of TCO properties of ZnO by silver addition. Superlattices Microstruct. **67**, 97–109 (2014)
21. Rajesh Kumar, Neeraj Khare, Temperature dependence of conduction mechanism of ZnO and Co-doped ZnO thin films. Thin Solid Films **516**, 1302–1307 (2008)
22. M. Yu, H. Qiu, X. Chen, H. Li, W. Gong, Al and Ni co-doped ZnO films with room temperature ferromagnetism, low resistivity and high transparence. Mater. Chem. Phys. **126**(3), 797–803 (2011)
23. R. Srivastava, Investigation on temperature sensing of nanostructured zinc oxide synthesized via oxalate route. J. Sens. Technol. **2**, 8–12 (2012)
24. C.C. Naik, A.V. Salker, Tailoring magnetic and dielectric properties of $Co_{0.9}Cu_{0.1}Fe_2O_4$ with substitution of small fractions of Gd3 + ions. J. Mater. Sci **29**(7), 5380–5390 (2017)
25. M.R. Bryce, M.C. Petty, Electrically conductive Langmuir-Blodgett films of charge-transfer materials. Nature **374**, 771–776 (1995)
26. A.A. Yousif, N.F. Habubi, A.A. Haidar, Nanostructure zinc oxide with cobalt dopant by PLD for gas sensor applications. J. Nano-Electron. Phys. **4**, 6 (2012)
27. S. Sharma, K. Nanda, R.S. Kundu, R. Punia, N. Kishore, Structural properties, conductivity, dielectric studies and modulus formulation of Ni modified ZnO nanoparticles. J. At. Mol. Condens. Nano Phys. **2**(1), 15–31 (2015)
28. M.M. Hassan, A.S. Ahmed, M. Chaman, W. Khan, A.H. Naqvi, A. Azam, Structural and frequency dependent dielectric properties of $Fe^{3+}$ doped ZnO nanoparticles. Mater. Res. Bull. **47**(12), 3952–3958 (2012)
29. C. Belkhaoui, R. Lefi, N. Mzabi, H. Smaoui, Synthesis, optical and electrical properties of Mn doped ZnO nanoparticles. J. Mater. Sci. **29**(8), 7020–7031 (2018)
30. M. Ashokkumar, S. Muthukumaran, Effect of Ni doping on electrical, photoluminescence and magnetic behavior of Cu doped ZnO nanoparticles. J. Lumin. **162**, 97–103 (2015)
31. M.M. Hassan, W. Khan, A. Azam, A.H. Naqvi, Influence of Cr incorporation on structural, dielectric and optical properties of ZnO nanoparticles. J. Ind. Eng. Chem. **21**, 283–291 (2015)
32. S. Sagadevan, K. Pal, Z.Z. Chowdhury, M.E. Hoque, Structural, dielectric and optical investigation of chemically synthesized Ag-doped ZnO nanoparticles composites. J. Sol-Gel Sci. Technol. **83**(2), 394–404 (2018)
33. R. Zamiri, A. Kaushal, A. Rebelo, J.M.F. Ferreira, Er doped ZnO nanoplates: synthesis, optical and dielectric properties. Ceram. Int. **40**, 1635–1639 (2014)